

The Rotation Period and Lightcurve Amplitude of Kuiper Belt Dwarf Planet 136472 Makemake (2005 FY9)

A. N. Heinze

Swarthmore College, 500 College Avenue, Swarthmore, PA 19081

`aheinze1@swarthmore.edu`

Daniel deLahunta

University of Rochester, 500 Joseph C. Wilson Blvd., Rochester, NY 14627

`ddelahun@mail.rochester.edu`

ABSTRACT

Kuiper Belt dwarf planet 136472 Makemake, formerly known as 2005 FY9, is currently the third-largest known object in the Kuiper Belt, after the dwarf planets Pluto and Eris. It is currently second only to Pluto in apparent brightness, due to Eris' much larger heliocentric distance. Makemake shows very little photometric variability, which has prevented confident determination of its rotation period until now. Using extremely precise time-series photometry, we find that the rotation period of Makemake is 7.7710 ± 0.0030 hours, where the uncertainty is a 90% confidence interval. An alias period is detected at 11.41 hours, but is determined with approximately 95% confidence not to be the true period. Makemake's 7.77 hour rotation period is in the typical range for Kuiper Belt objects, consistent with Makemake's apparent lack of a substantial satellite to alter its rotation through tides. The amplitude of Makemake's photometric lightcurve is 0.0286 ± 0.0016 magnitudes in V. This amplitude is about ten times less than Pluto's, which is surprising given the two objects' similar sizes and spectral characteristics. Makemake's photometric variability is instead similar to that of Eris, which is so small that no confident rotation period has yet been determined. It has been suggested that dwarf planets such as Makemake and Eris, both farther from the Sun and colder than Pluto, exhibit lower photometric variability because they are covered with a uniform layer of frost. Such a frost is probably the correct explanation for Eris. However, it may be inconsistent with the spectrum of Makemake, which resembles reddish Pluto more than neutrally colored Eris. Makemake may instead be a more Pluto-like object that we observe at present with a nearly pole-on viewing geometry – a possibility that can be tested with continuing observations over the coming decades.

Subject headings: Kuiper Belt, techniques: photometric, methods: data analysis

1. Introduction

The Kuiper Belt is interesting in several ways. It is a relatively unexplored region of our Solar System. It may have had profound effects on the rest of the Solar System, from influencing the migrations of the giant planets, to delivering impactors to Earth and the rest of the inner Solar System (Gomes et al. 2005). Its chemical and dynamical properties convey information about the formation and early evolution of the solar system. Finally, it is an analog to cold debris disks that are now being discovered by the Spitzer Space Telescope around other stars (Bryden et al. 2006).

Since even the largest Kuiper Belt objects can only be marginally resolved even by HST, photometric monitoring is an important tool for their study. For all objects it can reveal their shape and rotation period (Sheppard & Jewitt 2002; Ortiz et al. 2006). For larger objects such as Pluto it can indicate the distribution and color of surface albedo features. Over a period of decades, it can reveal the change in sub-Earth latitude, and possibly evidence of seasonal change in albedo features (Buratti et al. 2003). Information about shape and rotation constrains the impact history and physical properties (i.e. density and material strength) of the Kuiper Belt objects (Trilling & Bernstein 2006; Rabinowitz et al. 2006), which in turn provides tests of theories of solar system formation and early evolution. Information about color and albedo features, especially when combined with spectra, provides clues about the surface and atmospheric chemistry of the larger objects (Buratti et al. 2003; Brown et al. 2005; Licandro et al. 2006a).

This is an era of remarkable discoveries in the Kuiper Belt, with the three brightest known objects other than Pluto (136472 Makemake, 136108 Haumea, and 136199 Eris) all having been discovered within the last 6 years (see <http://www.gps.caltech.edu/~mbrown/planetlila/index.html>). Of these three, only Haumea has a confident published rotation period at present, and its rotational lightcurve, indicating a centrifugally elongated, highly ellipsoidal 1000 km object rotating once every 3.9 hours, makes it one of the most fascinating and bizarre objects in the solar system (Rabinowitz et al. 2006).

We present the first confident determination of the rotation period and rotational lightcurve amplitude of 136472 Makemake. In Section 2 we describe our observations, in Section 3 we detail our photometric reduction strategy, and in Section 4 we present our period determination methods and discuss the resulting periods. We discuss the implications of our results in Section 5, and we present our conclusions in Section 6.

2. Observations and Image Processing

In February 2006 we observed 136472 Makemake (then called 2005 FY9) in the U , V , and I -bands for four nights through bright moonlight using the 1.54 meter Kuiper Telescope. We were unable to determine the rotation period from these data, but the upper limits that we could set on the amplitude of the object's photometric variability suggested the project was very difficult.

Accordingly we applied for and received eight nights of lunar dark time in the spring of 2007. We experienced remarkably good weather, acquiring useful data on five nights in February and two in April. The 2007 data are so far superior to those from 2006 that we have based our lightcurve analysis only on our 2007 images.

We observed Makemake on the UT dates 2007 February 19, 21-23, and 26, and 2007 April 23-24, using the University of Arizona’s 1.54 meter Kuiper Telescope on Mt. Bigelow, just north of Tucson, AZ. Our instrument was the Mont4K CCD, a 4096 x 4096 pixel imager yielding a 9.7 arcminute square field of view. We used the CCD in 2x2 binning mode, obtaining a pixel scale of about 0.28 arcseconds/pixel. Our 2007 observations are summarized in Table 1.

Because our 2006 observations had shown the lightcurve amplitude to be very small, we planned our 2007 observations to obtain the largest possible amount of consistent, high-quality photometry. We spent a bare minimum of time on calibration stars during the time Makemake was observable each night, and used the *V* band almost exclusively to get a very large data set with consistent photometry. We used an integration time of 500 seconds, which yielded bright but un-saturated images of Makemake and appropriate comparison stars in the same field.

We processed our data using dark subtraction; flatfielding; correction of bad pixel regions; removal of cosmic rays using two iterations of our implementation of the laplacian edge detection algorithm described in the excellent work of van Dokkum (2001); and finally removal of isolated deviant (‘hot’) pixels (e.g. residuals from cosmic rays).

We paid special attention to the construction of our flat frames, because these were critical to the success of our photometric strategy. In the course of our observations we obtained both dome and twilight sky flats. Dome flats can be taken in large numbers and averaged to obtain extremely low noise. Conditions appropriate for taking sky flats occur only briefly, so averaged sky flats are always noisier. Dome flats, however, do not provide as reliable a measurement of the true illumination of the detector in real observing conditions. We processed our data using three different flat-fielding strategies: pure dome flats, pure sky flats, and composite flats. These last were constructed by first creating a sky/dome ratio image, then smoothing it, and then multiplying the original dome flat by the smoothed ratio, to produce a final image with the low noise of a dome flat but the correct illumination of a sky flat at low spatial frequencies. As expected, the dome flats produced substantially more scattered photometry than the other two strategies. The sky and composite flats produced very similar results, but the sky flats were slightly superior. We have therefore used images processed with sky flats throughout our analysis. Any flatfield gradients or other defects in the sky flats are observed to be far below what would be required to explain the observed variability of Makemake.

On the night of UT February 26, Makemake passed very close to two faint stars, which caused a spurious brightening of a few percent in our raw photometry. To solve this problem, we first stacked a large set of images on which Makemake was not close to the stars, obtaining a very low-noise image on which the faint stars could be accurately measured. Using this image, we found precise

values for the positions and brightnesses of the faint stars relative to a nearby, much brighter star. We then processed every Feb 26 image by subtracting an appropriately scaled and shifted version of the PSF of the brighter star on that image from the exact location of each of the faint stars we wished to remove. We tested the effectiveness of the subtraction by creating a new stacked image of the altered data. The stars had essentially vanished, as did the deviant signature in our Makemake photometry, leaving the Feb 26 data entirely consistent with the rest of our nights.

Figure 1 shows all the data from our observations on 2007 February 19, 21, 22, and 23 stacked to make a single image, with the path of Makemake appearing as four approximately colinear streaks moving toward the upper right.

3. Photometric Analysis

3.1. Acquiring the Relative Photometry

Our focus in this project was extremely accurate relative photometry. For each night, we identified a set of reference stars clearly visible on all images from that night. This set of reference stars was determined individually for each night, but because Makemake moves very slowly there was considerable overlap from one night to the next.

We obtained aperture photometry of all the reference stars and the science target. We tested the stars for variability by ratioing each to the sum of all the others, and calculating the normalized RMS scatter of the result. Since fainter stars ought to have a larger normalized scatter due to statistical photon noise and background noise, this normalized RMS should decrease monotonically as the brightness of the stars increases. Stars that deviated from this expected monotonic decrease were flagged as possible variables and, if the deviation was significant, removed from the reference star set. For most nights, extending this analysis to include Makemake itself resulted in its also being flagged as a variable ‘star’, as we would expect.

Having removed clear variables from our reference star set, we obtained relative photometry in which the brightness of Makemake was ratioed to the summed brightness of all the reference stars. There was a considerable overlap in reference star sets from one night to the next. This allowed us to make all the relative photometry in February, and all that in April, internally consistent with no guesswork. Doing this as accurately as possible was very important. Our first concern was to find the ratio of the summed flux over all the reference stars used in one night to the summed flux over all those used in the next night. As an example, we will take nights 1 and 2. Let i index images and j index stars in a given night, where F_{ij} will be the observed flux from star j on image i . Let s_1 represents the set of all reference stars for night 1, s_2 represents the same set for night 2, and s_{12} represents the subset of stars that were used for both night 1 and night 2. For each image i in night 1, we can then form the ratio:



Fig. 1.— This is a stacked image of the first four nights of the February data.

$$R_{1i} = \frac{\sum_{j \in s_1} F_{ij}}{\sum_{j \in s_{12}} F_{ij}} \quad (1)$$

Of course this simply ratios the sum over all reference stars used on night 1 to the sum only over those shared between nights 1 and 2. Now let \mathbf{R}_1 be the average of R_{1i} over all the images in night 1:

$$\mathbf{R}_1 = \overline{R_{1i}} \quad (2)$$

This \mathbf{R}_1 will then be an extremely accurate estimate of the true ratio of the summed flux of the two star sets s_1 and s_{12} . We can proceed similarly for night 2, letting i now index images in night 2 rather than night 1:

$$R_{2i} = \frac{\sum_{j \in s_2} F_{ij}}{\sum_{j \in s_{12}} F_{ij}} \quad (3)$$

And, again, \mathbf{R}_2 will be an average over all the images in night 2:

$$\mathbf{R}_2 = \overline{R_{2i}} \quad (4)$$

Now we define a new ratio:

$$\mathbf{C}_2 = \frac{\mathbf{R}_2}{\mathbf{R}_1} \quad (5)$$

\mathbf{C}_2 is of course the ratio of the summed flux over all night 2 reference stars (the set s_2) to the summed flux over all night 1 reference stars (the set s_1). It has been constructed exclusively using the ratios of stellar fluxes measured on the same images. The effects of seeing, airmass, and atmospheric transparency variations cancel out, yielding a remarkably precise value.

We have shown how we can precisely measure the ratio of the summed flux of all reference stars used on night 2 to that of all reference stars used on night 1, assuming the sets overlap somewhat. In general, there was extensive overlap, well over 50%. Of course, there might be little or no overlap between, say, the first night and the fifth night. Rather than trying to establish the ratio of reference star sums across such a large gap directly, we calculated them exclusively from one night to the next, so that, e.g. \mathbf{C}_3 was the ratio of the sum over stars used on night 3 to those used on night 2, \mathbf{C}_4 was the ratio of stars from night 4 to stars from night 3, etc. Finally, the relative photometry for the target from, say, image i on night k was calculated by:

$$T_i = \left(\frac{F_{targ,i}}{\sum_{j \in s_k} F_{ij}} \right) \cdot \prod_{n=2}^{n=k} \mathbf{C}_n \quad (6)$$

Here, of course, i indexes images in night k , j indexes stars in the reference star set for night k , and n indexes nights. $F_{targ,i}$ is the flux from Makemake on image i of night k , and T_i is the final relative photometry result for Makemake on image i . This procedure gave us a consistent scaling for all the photometry from February, and all that in April, assuming the reference stars were non-variable (as we had already tested), but making no assumptions about the brightness of Makemake itself. The longer gap between the February and April data was bridged using images of the April field taken during our February run, under excellent weather conditions when both fields were high in the sky. The February-April bridge was the only step where we had to use a ratio of two sets of stars that were not both measured on the same images. A larger aperture was used for this final ratio, to minimize the effects of seeing variations between the different images. Our final step was simply to normalize the relative photometry.

3.2. Selecting the Final Aperture and Reference Stars

We used a photometric aperture of 13.0 pixel (3.6 arcsecond) radius for our first-pass relative photometry of Makemake. We constructed a Lomb-Scargle periodogram of this preliminary data set using the routine `period.c` from Press et al. (1992). This routine identified clear sinusoidal signals at about 5.9, 7.8, and 11.4 hour periods. These values are consistent with a true 7.8 hour period flanked by positive and negative diurnal aliases. We made folded lightcurves at each period, and found that the 7.8 hour period also showed the lowest scatter. We adopted this period as our preliminary model. We tried different photometric apertures, and found that an aperture of 10.5 pixel (2.9 arcsecond) radius minimized the scatter from the 7.8 hour sinusoidal fit. We adopted this as our aperture for our final photometric analysis.

We experimented with different subsets of our initial selection of non-variable reference stars. One concern was that reference stars of different colors might introduce systematics into our relative photometry, due to the color-dependent extinction of Earth’s atmosphere. We had acquired a few B band images each night, and so were able to obtain the $B - V$ colors of our reference stars. Our investigation showed no evidence of measurable color-dependent atmospheric extinction, so we can be confident that this is not a source of systematic error in our photometry. From ten semi-random trials with different subsets of reference stars, we chose the subset that produced the lowest scatter from the 7.8 hour sinusoidal fit for our final photometric analysis. The majority of bright ($V < 17.0$) stars present in the initial non-variable sample were included in this final, optimized set.

For several reasons, our choice of a 7.8 hour period sinusoid as our standard model for determining the optimal reference star set is unlikely to have meaningfully biased the final data in favor of this period. First, we had already screened the reference stars for variability before the initial determination of the period, and the final set of reference stars we adopt includes the majority of bright stars identified as non-variable at first. Also, a 7.8 hour period with a sinusoidal variation appears clearly for every reasonable choice of aperture and reference star set, and it appears in both the February and April data when these are analyzed separately. Our tuning of the photometric

aperture and the reference star set simply reduced the random scatter in the final photometry.

Table 2 and Figures 2 and 3 present our final photometry, as optimized by the process above. The figures present photometry after correction for changes in the Sun-object-Earth phase angle, the geocentric and heliocentric distances, and the light travel time; the table presents uncorrected values. We have used distance information from the Minor Planet and Comet Ephemeris Service (<http://www.cfa.harvard.edu/iau/MPEph/MPEph.html>) in applying these corrections. Figure 2 shows our February 2007 photometry data, with sinusoidal fits at the 5.9, 7.77, and 11.4 hour periods. Figure 3 presents the data and fits for April 2007. The figures support our initial impression that 7.77 hours is the true period, while the others are diurnal aliases in which either one too few or one too many cycles occur during the diurnal gaps in our observations.

3.3. Phase Slope

Our measurements were timed near opposition to get the longest possible observing time per night and optimize our ability to constrain the period. For this reason, they do not span a large range in Sun-object-Earth phase angle: the range is only 0.59° to 0.84° . However, our photometry is sufficiently accurate to derive a meaningful phase slope: 0.037 ± 0.013 mag/ $^\circ$. This agrees with the result of Rabinowitz et al. (2007), who found a slope of 0.054 ± 0.019 mag/ $^\circ$. These measurements fit well into the overall pattern of shallow phase slopes for large KBOs and steeper slopes for small ones (Rabinowitz et al. 2007). For comparison, the *V*-band phase slope of Pluto is 0.032 ± 0.001 mag/ $^\circ$ (Buratti et al. 2003), that of Eris has been measured at 0.105 ± 0.020 mag/ $^\circ$ (Rabinowitz et al. 2007) and 0.09 ± 0.03 mag/ $^\circ$ (Sheppard 2007), and that of Haumea is 0.110 ± 0.014 mag/ $^\circ$ (Rabinowitz et al. 2007). The phase slopes of smaller KBOs are typically considerably steeper, ranging up to about 0.25 mag/ $^\circ$ (Rabinowitz et al. 2007). Figure 4 shows our data, after correction for changing geocentric distance and the subtraction of a smoothed model of the rotational lightcurve, plotted against Sun-object-Earth phase angle.

3.4. Tests for Long Term Variability

In addition to acquiring the relative photometry we have discussed above, we observed Landolt standard star fields to obtain a calibration for absolute photometry. Magnitudes for our on-chip reference stars based on this calibration are given in Tables 3 and 4. All moderately prominent stars that passed our variability tests are shown on these tables, even if they were not used in the final relative photometry. We include these tables to provide a perspective on the brightness and number of on-chip reference stars required for relative photometry of the precision we have attained, and to make clear which stars we rejected and which we chose for the final relative photometry.

Based on our Landolt calibration, we find that the average *V*-band magnitude of Makemake is 17.238 ± 0.029 , standardized to Sun-object-Earth phase angle 0.8° , geocentric distance 51.324

Table 1: Observing Log

UT Date	# Useful Images	Seeing FWHM
2007 Feb 19	29	2.1 asec
2007 Feb 21	38	2.4 asec
2007 Feb 22	28	2.1 asec
2007 Feb 23	41	1.5 asec
2007 Feb 26	50	1.7 asec
2007 Apr 23	38	1.2 asec
2007 Apr 24	46	1.8 asec

Table 1: The number of useful images includes only 500 second science exposures targeting Make-make that were included in the final photometric analysis. Seeing limits are based on the FWHM of stars on one randomly chosen image from near the middle of the observing sequence on each night, measured with the IRAF imexam task.

Table 2: Relative Photometry

Time (hrs)	Relative flux	heliocentric distance (AU)	geocentric distance (AU)	phase (degrees)
4.896878	0.994717	51.98382243	51.1880694	0.651377632
5.048531	0.992775	51.98382344	51.18803212	0.651322416
5.200008	0.986414	51.98382445	51.18799488	0.651267265
5.361675	1.006923	51.98382552	51.18795514	0.651208403
5.513006	1.00167	51.98382652	51.18791793	0.651153305
5.664145	1.002119	51.98382753	51.18788078	0.651098276
5.827528	1.017613	51.98382861	51.18784061	0.65103879

Table 2: Time is measured from 00:00 UT Feb 19, 2007 and is not corrected for light travel time. Flux is not corrected for distance or phase. Table 2 is available in its entirety only online: a sample is provided here as a guide to its form and content.

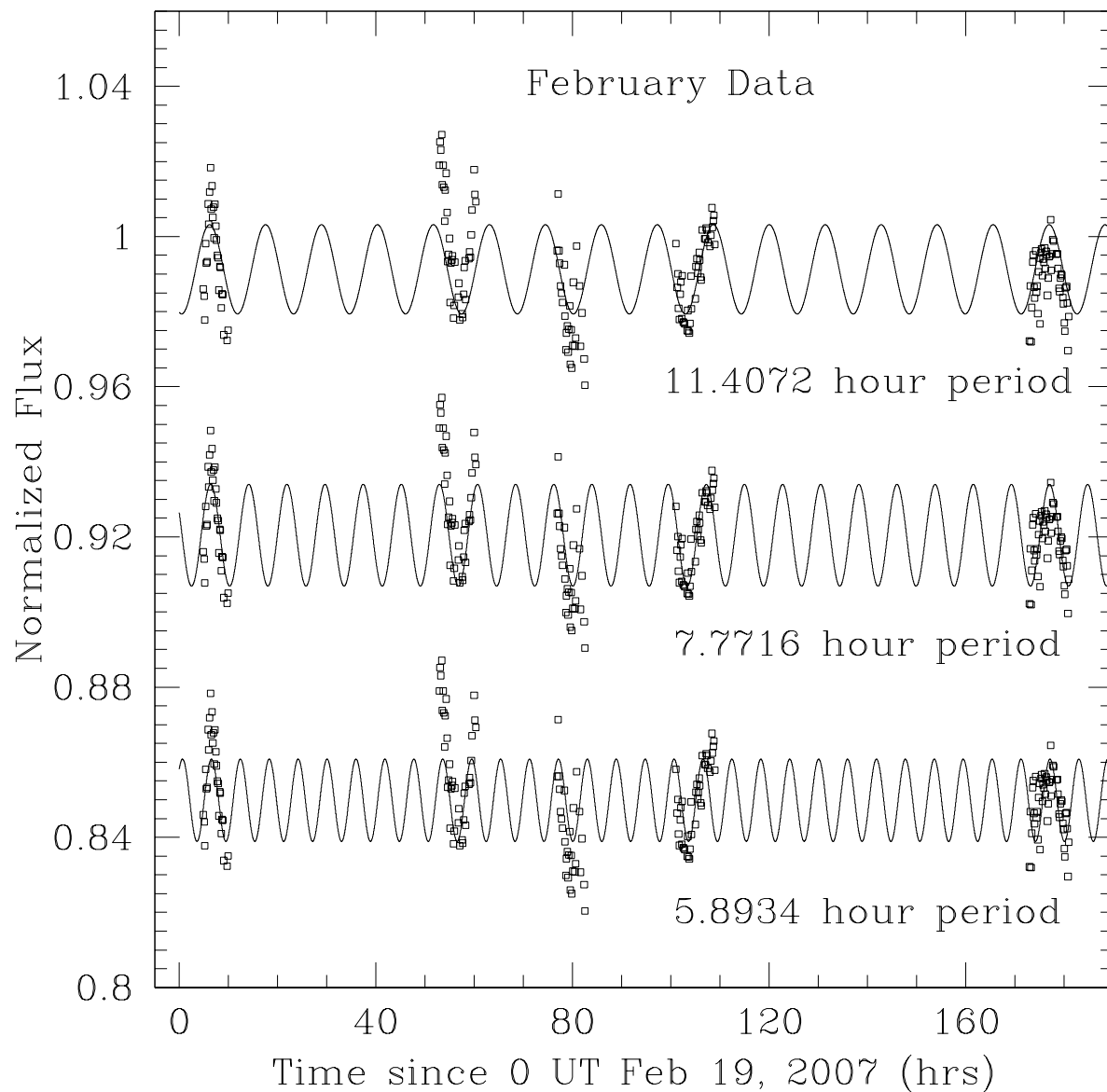


Fig. 2.— Time series photometry from 2007 Feb 19, 21, 22, 23, and 26, corrected for phase angle and geocentric and heliocentric distance, and showing sinusoidal fits at 5.9, 7.77, and 11.4 hour periods. Normalized relative photometry is shown, with the data and fits for the 7.77 and 5.9 hour periods offset for clarity.

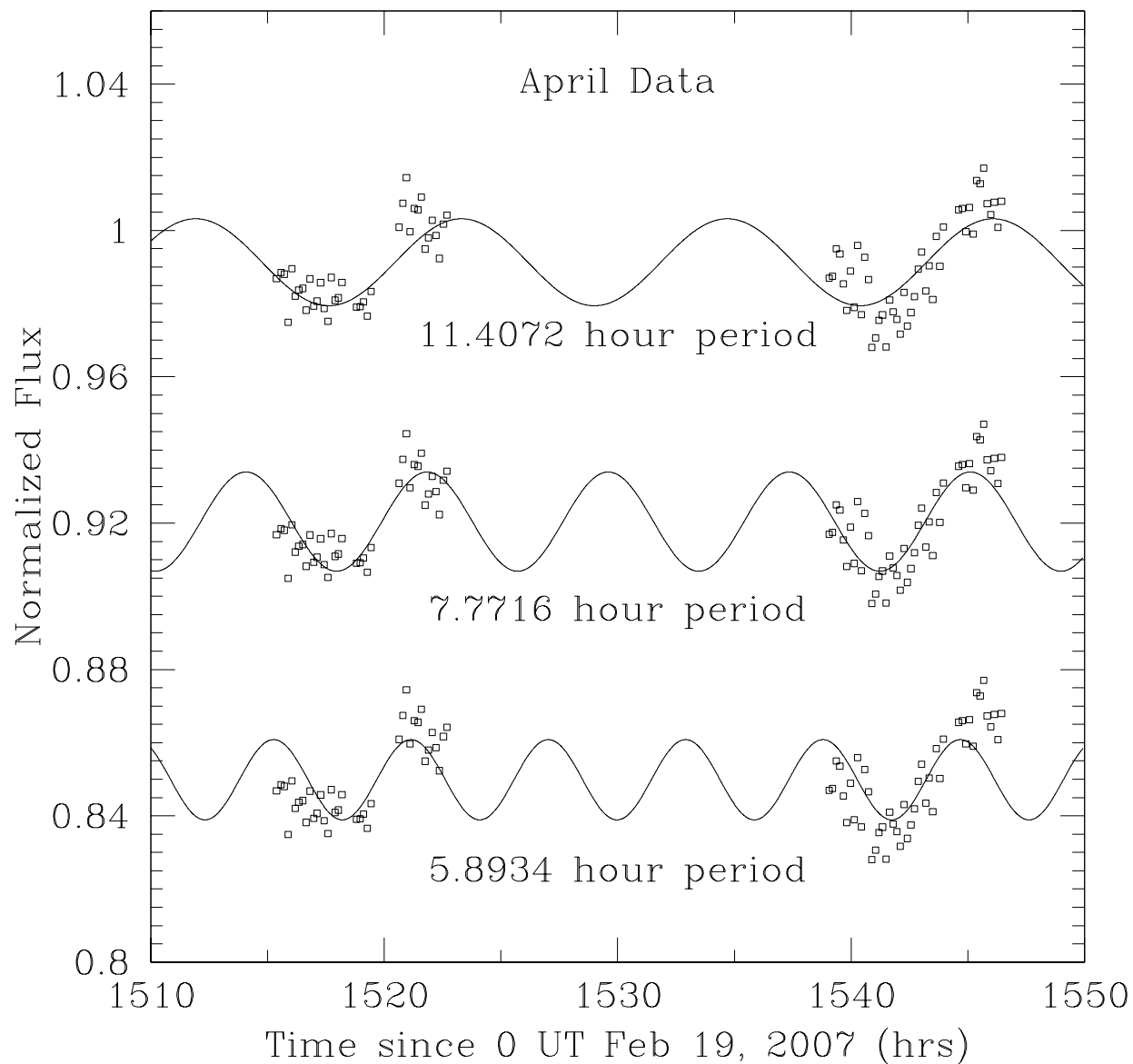
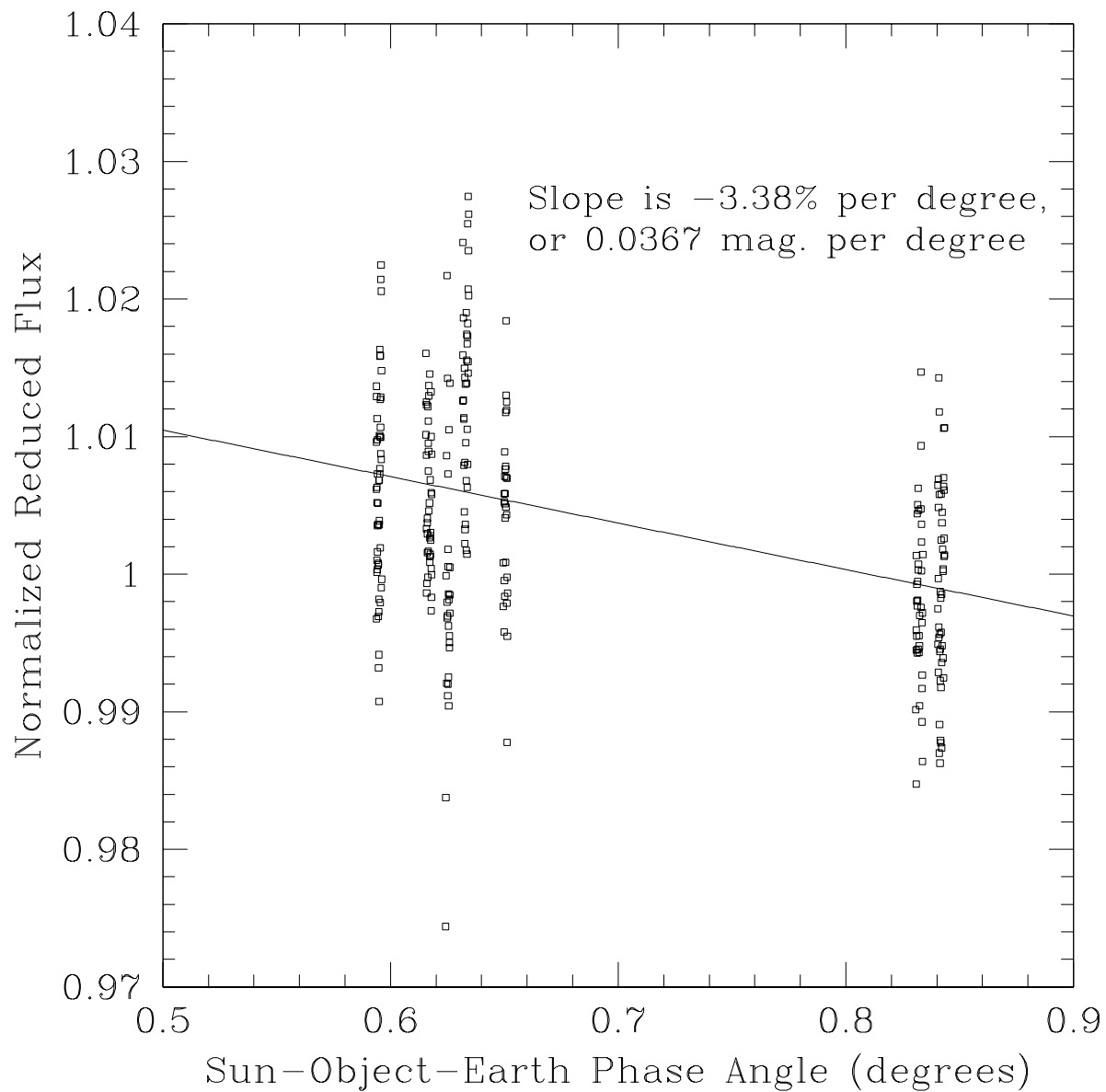


Fig. 3.— Time series photometry from 2007 Apr 23 and 24, corrected for phase angle and geocentric and heliocentric distance, and showing sinusoidal fits at 5.9, 7.77, and 11.4 hour periods. Normalized relative photometry is shown, with the data and fits for the 7.77 and 5.9 hour periods offset for clarity.



AU, and heliocentric distance 51.994 AU. This corresponds to a V band absolute magnitude of 0.079 ± 0.031 , standardized to a phase angle of 0.0° assuming there is no opposition surge at phase angles smaller than we have measured. This can be compared with the absolute V magnitude from Rabinowitz et al. (2007): 0.091 ± 0.015 , based on observations from 2005 April 4-23. Our 2006 observations of Makemake showed its average magnitude to be 16.419 ± 0.030 in the I-band, 17.246 ± 0.027 in the V-band, and 18.359 ± 0.074 in the U-band, at a geocentric distance of 51.204 AU, a heliocentric distance of 51.922 AU, and a Sun-object-Earth phase angle of 0.8 degrees. We can transform our 2007 V magnitude to match these phase and distance parameters: the result is 17.232 ± 0.029 . Comparison of our 2007 result with both the 2005 measurements of Rabinowitz et al. (2007) and our own 2006 result shows that the rotationally averaged brightness of Makemake has remained constant to within measurement uncertainty over this two year period.

4. Period Identification

To make our final analysis of periodic variations in the photometry of Makemake, we used photometry from the optimized aperture and reference star set discussed in Section 3.2 above. These data are also plotted in Figures 2 and 3. This data set was corrected for Makemake’s changing Sun-object-Earth phase angle and heliocentric and geocentric distances. We also applied a light-travel-time adjustment to our photometric timing.

The second line from the top in Figure 5 shows the Lomb-Scargle periodogram for our final data set. Clear peaks with vanishingly small false-alarm probability are seen at a period of 7.7716 hours and at diurnal aliases of 5.8934 and 11.4072 hours, with the latter alias being much the stronger of the two. There is no evidence for the 11.24 hour periodicity suggested by Ortiz et al. (2007). To test if the strong 11.4 hour alias might actually be the true period, we created synthetic data sets with the same time sampling as our real data, but with the actual photometry replaced with values from sinusoidal fits to our data at the 7.7716 hour and 11.4072 hour periods, plus pure gaussian noise with $\sigma = 0.9\%$. The top line and the line third from the top in Figure 5 are the periodograms from these two synthetic data sets. The relative strengths of the different peaks in the real data match excellently with those from the synthetic data with a 7.77 hour period, and do not match those from the 11.4 hour synthetic data set.

We also analyzed our data set using the Phase Dispersion Minimization (PDM) method (Stellingwerf 2007), which, unlike the Lomb-Scargle periodogram, does not assume that the data will be approximately sinusoidal. The PDM method scans a broad, finely sampled range of periods, and identifies the one producing the minimum dispersion, parametrized by the θ statistic, which is a measure of the deviation of the actual data from a smoothed lightcurve folded to the given period. To make this smoothed lightcurve one first folds the data and then smooths it using a sliding boxcar average over a fixed fraction of the period. The length of our boxcar was 0.2 periods: this was the shortest value that gave clean, non-jagged curves.

Table 3: February Reference Stars

GSC 2.3 Name	α	δ	V mag	B-V mag	Nights Used				
	h:m:s	d:m:s			2/19	2/21	2/22	2/23	2/26
N5B8001928	12:26:10.3	+29:31:33.4	15.00	0.54	Y	Y	Y	Y	-
N5B8001857	12:26:26.3	+29:29:48.4	15.67	0.59	Y	Y	-	-	-
N5B8001920	12:26:27.8	+29:31:19.4	18.56	1.48	Y	Y	-	-	-
N5B8002052	12:26:25.7	+29:39:04.5	17.40	0.53	Y	Y	-	-	-
N5B8001845	12:25:59.9	+29:29:41.7	15.67	1.09	Y	Y	Y	Y	-
N5B8001861	12:26:06.1	+29:29:58.5	17.98	1.12	Y	Y	Y	Y	-
N5B8002205	12:26:25.7	+29:36:25.5	18.02	0.93	-	Y	-	-	-
N5B8002220	12:26:13.7	+29:37:31.4	17.71	0.59	-	Y	-	-	-
N5B8002173	12:25:54.5	+29:36:45.8	19.35	0.69	-	Y	Y	Y	Y
N5B8002059	12:25:47.8	+29:34:30.0	19.44	0.29	-	Y	Y	Y	Y
N5B8000046	12:25:36.1	+29:33:49.6	14.66	0.63	-	-	Y	Y	Y
N5B8001929	12:25:33.0	+29:31:44.1	16.63	0.90	-	-	Y	Y	Y
N5B8002118	12:25:31.6	+29:35:50.2	17.96	0.70	-	-	Y	-	Y
N5B8002064	12:25:36.1	+29:34:38.5	15.96	0.29	-	-	Y	Y	Y
N5B8001803	12:26:04.9	+29:28:41.7	16.65	0.71	-	-	-	Y	-
N5B8002145	12:25:28.2	+29:36:16.5	16.89	0.73	-	-	-	-	Y
N5B8002034	12:25:24.7	+29:33:56.9	17.58	1.03	-	-	-	-	Y
N5B8001952	12:25:25.3	+29:32:19.5	17.93	1.36	-	-	-	-	Y
N5B8001864	12:26:25.5	+29:29:58.1	16.27	1.29	-	-	-	-	-
N5B8001918	12:26:29.2	+29:31:14.0	18.21	...	-	-	-	-	-
N5B8002089	12:26:19.2	+29:35:01.2	16.99	0.67	-	-	-	-	-
N5B8001940	12:25:57.1	+29:31:52.4	16.87	0.64	-	-	-	-	-
N5B8001893	12:26:05.8	+29:30:38.4	18.97	0.42	-	-	-	-	-
N5B8002196	12:26:05.7	+29:37:11.4	18.65	0.63	-	-	-	-	-
N5B8002177	12:25:58.4	+29:36:50.5	19.18	0.65	-	-	-	-	-
N5B8002038	12:25:50.8	+29:33:58.2	19.24	1.53	-	-	-	-	-
N5B8001852	12:25:50.7	+29:29:52.6	16.30	0.98	-	-	-	-	-
N5B8001820	12:25:39.9	+29:29:16.1	15.58	0.63	-	-	-	-	-
N5B8001816	12:26:05.0	+29:29:03.5	18.75	1.34	-	-	-	-	-
N5B8002072	12:25:40.9	+29:34:53.8	18.92	0.84	-	-	-	-	-
N5B8002060	12:25:44.9	+29:34:33.1	18.76	0.97	-	-	-	-	-
N5B8002245	12:25:25.0	+29:38:15.7	19.41	1.16	-	-	-	-	-
N5B8002232	12:25:32.1	+29:37:57.7	19.22	1.48	-	-	-	-	-
N5B8002201	12:25:34.5	+29:37:20.4	18.63	0.43	-	-	-	-	-
N5B8002103	12:25:36.2	+29:35:24.5	19.32	1.35	-	-	-	-	-

Table 3: Columns 1-3 were obtained using the GSC 2.3 catalog. We identified our stars on this catalog using a search on the VizieR website. Right ascension and declination are in terms of J2000.0 coordinates. V and $B - V$ magnitudes were determined from our own data. The magnitudes and colors have uncertainties of about 0.03 and 0.07, respectively; or somewhat larger for the faintest stars. The nights that that star were used in photometry are shown in the last five columns.

Table 4: April Reference Stars

GSC 2.3 Name	α	δ	V mag	B-V mag	Nights Used	
	h:m:s	d:m:s			4/23	4/24
N57S005224	12:21:58.9	+29:59:00.5	14.83	1.14	Y	Y
N57S000009	12:21:48.8	+29:53:34.0	14.68	0.77	Y	Y
N57S005246	12:21:43.1	+30:00:21.6	18.76	1.34	Y	Y
N5B8003796	12:22:11.1	+29:59:58.0	18.20	0.84	Y	Y
N5B8003678	12:22:15.4	+29:58:23.3	14.92	1.01	Y	Y
N57S005147	12:22:17.2	+29:55:30.1	17.49	0.85	Y	Y
N57S000001	12:21:38.3	+29:59:58.1	13.71	...	-	Y
N57S005090	12:21:50.0	+29:53:58.9	15.83	1.50	-	-
N57S005066	12:21:44.0	+29:53:08.7	18.51	0.22	-	-
N57S005222	12:21:46.7	+29:58:56.9	15.16	0.96	-	-
N5B8003805	12:22:08.1	+30:00:03.8	18.82	0.72	-	-
N57S005196	12:22:13.0	+29:57:26.9	17.18	1.25	-	-
N57S005181	12:22:12.9	+29:56:54.3	18.58	1.11	-	-
N57S005167	12:22:07.2	+29:56:16.9	18.91	1.45	-	-
N5B8003925	12:22:02.4	+30:01:18.9	16.07	1.22	-	-

Table 4: Columns 1-3 were obtained using the GSC 2.3 catalog. We identified our stars on this catalog using a search on the VizieR website. Right ascension and declination are in terms of J2000.0 coordinates. V and $B - V$ magnitudes were determined from our own data. The magnitudes and colors have uncertainties of about 0.03 and 0.07, respectively; or somewhat larger for the faintest stars. The nights that that star were used in photometry are shown in the last two columns.

The results of applying the PDM method to our data and to the two synthetic data sets previously discussed are shown in the top three curves of Figure 6. Again, the 7.77 hour period is strongly favored, and the 11.4 hours synthetic data does not reproduce the observed relative amplitudes of the different peaks. The real data shows a strong peak at 15.54 hours, which is twice the dominant period and corresponds to a double-peaked lightcurve. The highest peak near 11 hours has shifted to 11.6878 hours, rather than 11.4072 as in the periodogram. This 11.69 hour period was not seen in the periodogram because the resulting lightcurve is strongly non-sinusoidal. The fact that the same peak appears in the synthetic 7.77 hour data suggests it is an artifact of the sampling. The highest peaks near 7.77 and 11.4 hours in the PDM diagram are not significantly shifted from the same peaks in the periodogram analysis.

Our dominant peak near 7.77 hours is divided into many sub-peaks separated by about 0.04 hours, which correspond to different integer numbers of periods elapsing between our February and April observing runs. This is shown in Figure 7. The peak at 7.73 hours is very close in amplitude to the dominant peak in the periodogram, but the PDM analysis is decisive in preferring the 7.77 hour peak.

Even with our careful night-to-night calibration, flatfield errors and other effects could potentially impose slight night-to-night shifts in our photometry. Surprisingly, shifts of this type can move power from one peak to another in a periodogram or PDM analysis (Ortiz 2009, private communication). Accordingly, we calculated the average nightly offsets from our best fit smoothed model, and found an RMS average offset of 0.442%. We performed a Monte Carlo simulation in which random offsets following a gaussian distribution with $\sigma = 0.442\%$ were added to each night of our real data. The Monte Carlo simulation involved 1,000 realizations, each of which was analyzed with both the periodogram and the PDM techniques.

The periodogram analysis preferred a period near 7.77 hours in 76.5% of cases, a period near 7.73 hours in 18.4% of cases, and a period near 11.4 hours in 4.8% of cases. It gave bizarre and unreasonable results in 0.3% of cases. The PDM analysis gave a period near 7.77 hours in 91.6% of cases, a period near 7.73 hours in 0.2% of cases, a period near 11.4 hours in 6.3% of the cases, and other period in 1.9% of cases. The lowest line in Figures 5 and 6 is from one of the rare realizations in this Monte Carlo simulation where the 11.4 hour period was preferred. Note that even in this case, the peaks do not match well with the 11.4 hour synthetic data: in particular, the 5.9 hour alias is too strong.

In only 4.8% of cases did both PDM and periodogram methods yield a period near 11.4 hours. Since the 7.77 hour period is preferred by both methods in the real data set, it appears we can rule out the 11.41 hour period at roughly the 95.2% confidence level based on this experiment. The PDM method should be sensitive to any real periods in the data. Since it finds a 7.73 hour period in only 0.2% of cases, it also seems unlikely that this can be the real period.

Ortiz et al. (2007) carried out a program of intensive photometry on Makemake similar to our own. They preferred a period of 11.24 hours, but peaks near 11.41 and 7.8 hours do appear in

their Figure 1, with the 11.41 hour peak specifically mentioned in the caption. Thus there is an indication of the dominant period we detect in their data as well.

To complete our analysis, we present in Table 5 a list of all the periods that have been considered for Makemake: the 7.77 hour dominant period, the 7.73 and 11.41 hour periods we have already largely dismissed, the 11.24 hour period preferred by Ortiz et al. (2007), the 11.69 hour period identified in our PDM analysis, and the 15.542 hour double-peaked period from our PDM analysis.

In Figures 8 through 12, we compare the folded lightcurve at our dominant period of 7.77 hours against lightcurves constructed from our data folded at different periods. In every case the lightcurve is fit by a smoothed model such as is used in the PDM analysis, and the RMS scatter from this model is given. A total of 1.5 periods are shown to allow examination of any possible discontinuity.

Figure 8 compares our dominant lightcurve with the strong alias at 11.41 hours. We have already argued based on the Monte Carlo simulation that this period is ruled out at the 95% confidence level; visually, as well as mathematically, the fit is decidedly poorer.

Figure 9 compares the dominant period with the sub peak at 7.73 hours. In the Monte Carlo simulation, the 7.73 hour result was found in 18.4% of cases by periodogram analysis, but only in 0.2% of cases by PDM analysis. The figure suggests a reason: the 7.73 hour lightcurve approaches a perfect sinusoid more closely than the 7.77 hour version. Since there is no reason why the PDM analysis would miss a valid period in 99.8% of cases, it seems clear that the periodogram’s frequent identification of the 7.73 hour period is due to the true lightcurve’s having an imperfectly sinusoidal shape, thereby shifting some power away from the true 7.77 hour period in the periodogram analysis, but not in the PDM analysis since the latter has no problem with non-sinusoidal curves. This is consistent with Figure 7.

Figure 10 compares the 7.77 hour lightcurve with one from the 11.24 hour period preferred by Ortiz et al. (2007). There is no evidence for this period in our data, and the fit, as expected, is very poor. We have already noted that 7.8 and 11.41 hour peaks indicative of the true period and its alias exist in the periodogram of Ortiz et al. (2007).

Figure 11 compares the 7.77 hour result against a lightcurve folded at the strange period of 11.69 hours which was stronger than the 11.41 hour alias in the PDM analysis. The jagged appearance of the smoothed curve, together with a striking disagreement between the Feb 19 and Feb 26 data, clearly indicate that this period is unphysical. The specific sequence of gaps in our data set has evidently permitted this odd folding to have a formally low RMS, but it clearly cannot represent a real period. This is supported by the observation in Figure 6 that the 11.69 hour peak appears even in the data that simulate a perfect 7.77 hour sinusoid.

Finally, Figure 12 explores the possibility that the true period might be twice our preferred value of 7.77 hours: that is, that the lightcurve is double-peaked. Folding with this period produces

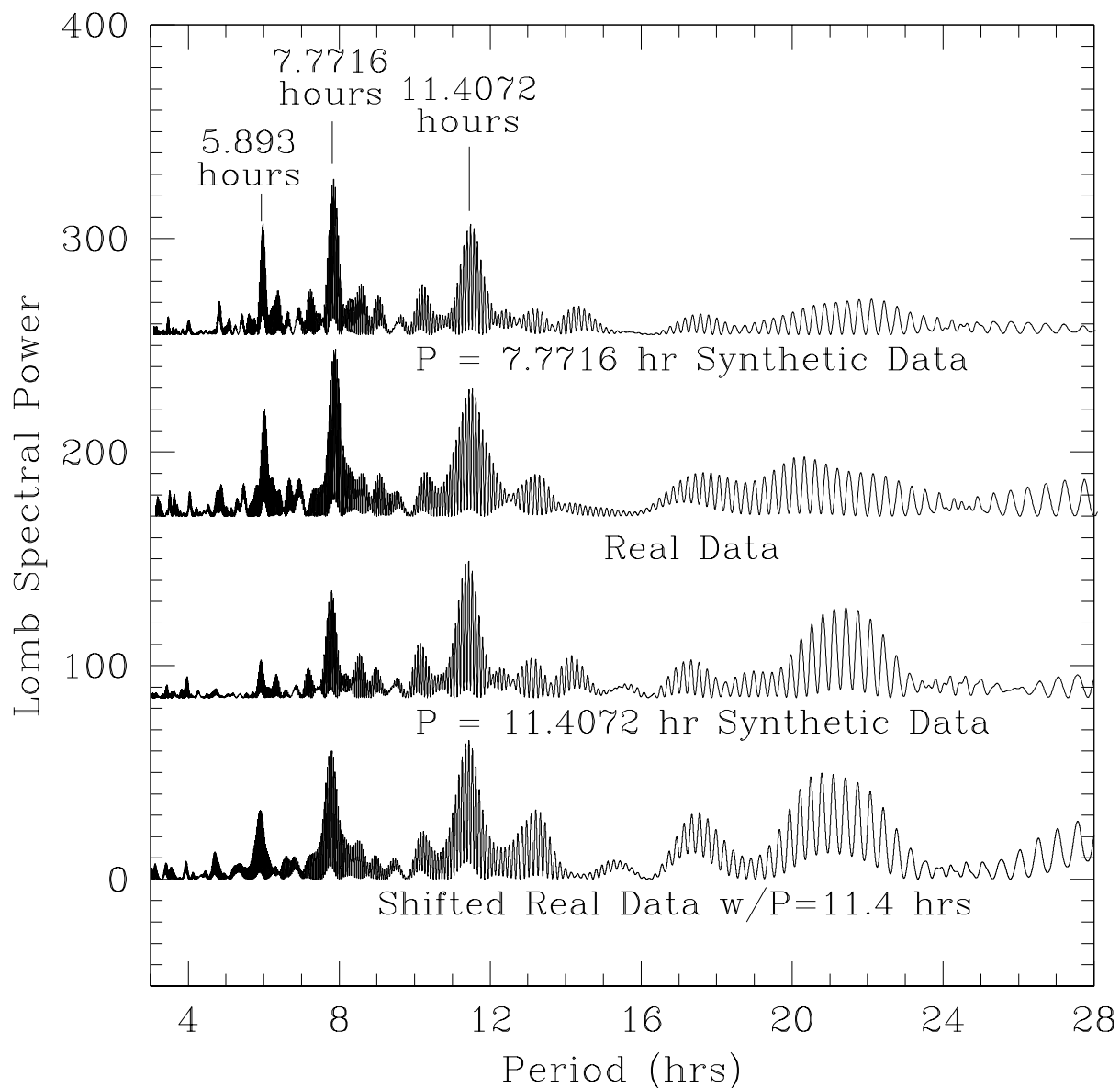


Fig. 5.— Lomb-Scargle periodogram power of our real data, two synthetic data sets, and a shifted version of our real data from the Monte Carlo simulation, chosen to be one of the rare cases where the 11.4 hour period was preferred. The four periodograms are offset for clarity. The pattern of peaks in the synthetic data set with the 7.77 hour period matches that for the real data much better than the other.

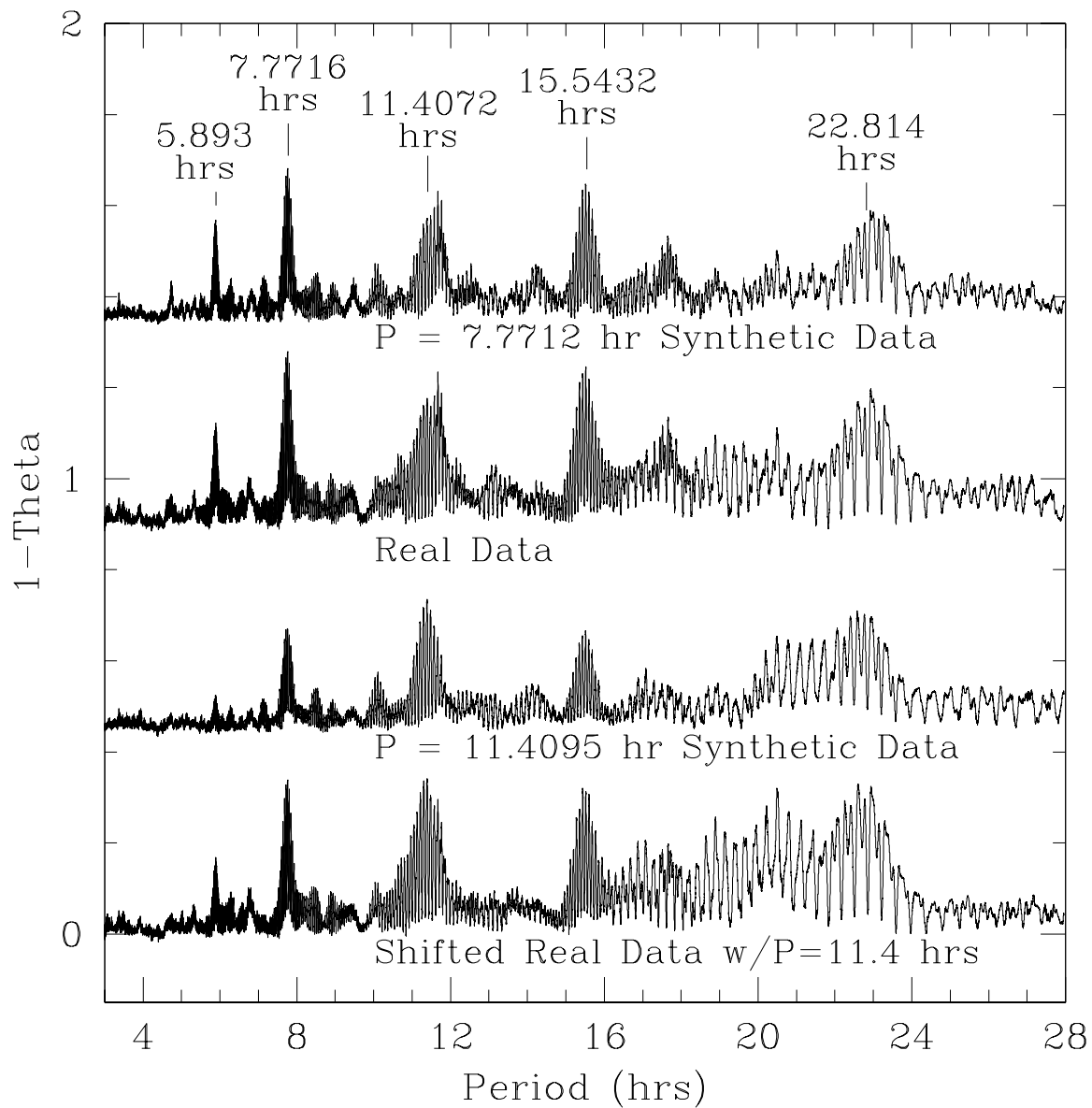


Fig. 6.— Phase Dispersion Minimization method of our real data, two synthetic data sets, and a shifted version of our real data from the Monte Carlo simulation, chosen to be one of the rare cases where the 11.4 hour period was preferred. The four periodograms are offset for clarity. The pattern of peaks in the synthetic data set with the 7.77 hour period matches that for the real data much better than the other.

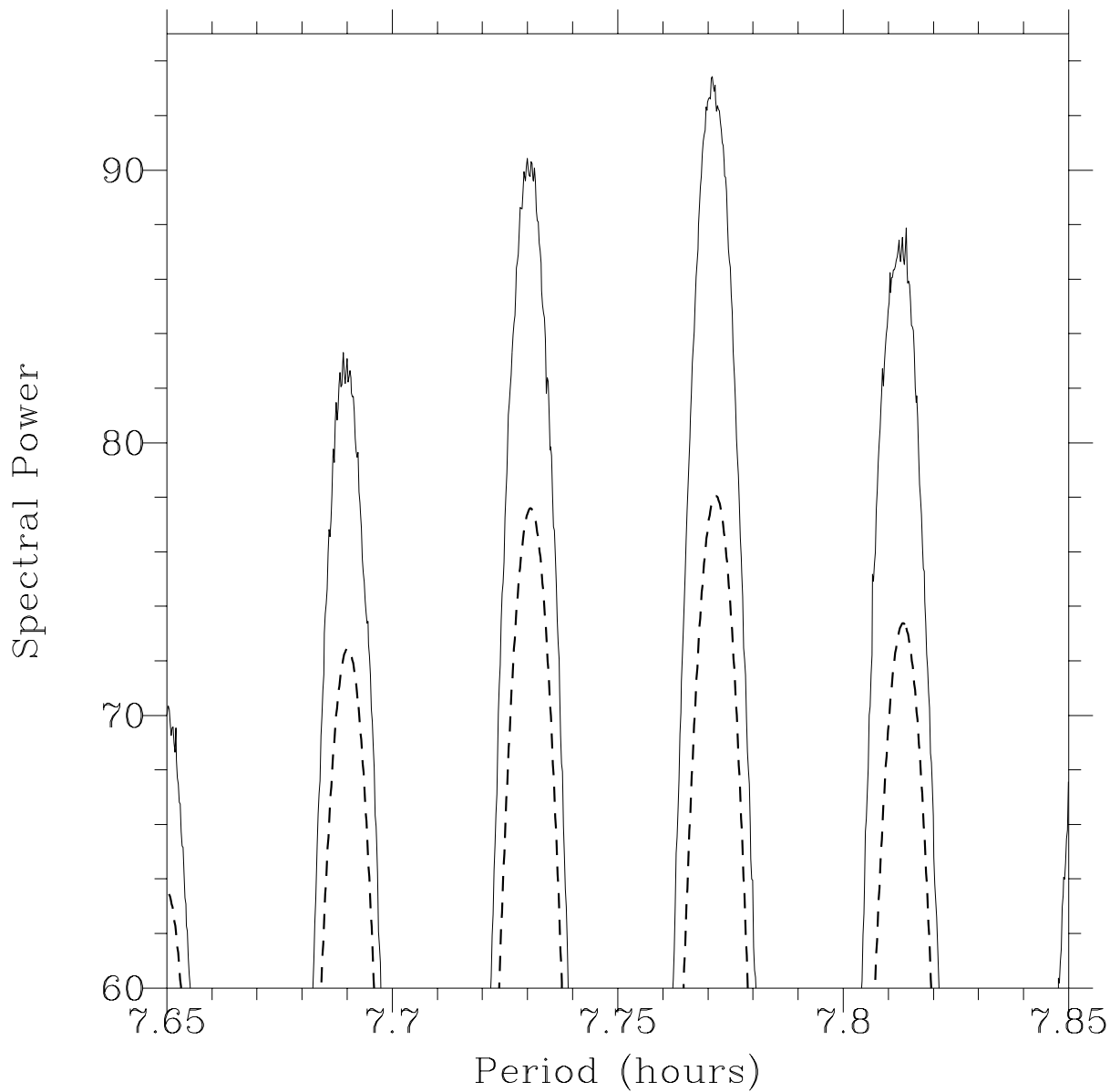


Fig. 7.— Scaled $(1 - \theta)$ value from the PDM analysis (solid line) and periodogram power (dashed line) from our real data, zoomed in on the dominant peak near 7.77 hours. The periodogram is not completely decisive between the 7.77 hour peak and the sub peak at 7.73 hours, but the PDM analysis strongly favors the 7.77 hour peak.

Table 5: Possible Periods

Period (hrs)	ID Method	RMS (Smoothed Fit)	RMS (Sine Fit)	PDM $1-\theta$ Value	Periodogram Power
5.8934	Periodogram	0.010013	0.010046	0.2117	49.96
7.7306	Periodogram	0.008093	0.008255	0.3626	77.59
7.7710	PDM	0.007904	0.008237	0.3792	77.87
7.7716	Periodogram	0.007924	0.008224	0.3778	78.06
11.24	Ortiz et al.	0.009871	0.010054	0.2253	49.49
11.4072	Periodogram	0.009330	0.009427	0.2654	59.80
11.4100	PDM	0.009234	0.009436	0.2768	59.37
11.6878	PDM	0.008543	0.010472	0.3356	37.71
15.5420	PDM	0.008331	0.012624	0.3468	1.43
15.5432	Periodogram	0.008357	0.012622	0.3450	1.47

Table 5: Here we present various possible periods and aliases thereof. Though the differences are insignificant, the preferred periods of both the periodogram and PDM methods are shown in cases where each had a prominent peak. The 15.54 hour ‘Periodogram’ period is simply double the 7.77 hour periodogram result: there was no actual peak in the diagram at this point. The Lomb-Scargle Periodogram looks for sinusoidal signals, so in addition to the periodogram power we have included the RMS deviation from the best-fit sinusoid at each period. The 15 hour periods are double-peaked, so the sine fit RMS for them indicates the RMS from a model that does not fit the data at all. The PDM method compares the data to a smoothed curve. The larger the $1-\theta$ statistic is, the better the PDM fit. Periods near 7.771 hours are favored by all measures.

a clean, low-scatter lightcurve, as indeed it must, but the degree of symmetry is improbable. The twin peaks are very similar and spaced almost exactly 0.5 periods apart. While it is impossible absolutely to rule out a remarkably symmetrical albedo distribution that could produce such a double-peaked lightcurve, it is far more likely that 7.77 hours is the true period and the lightcurve is single-peaked.

Finally, we conclude at the 95% confidence level that the true period is near 7.77 hours. Based on the PDM results from our Monte Carlo simulation, we quote a value of 7.7710 ± 0.0030 hours, where the uncertainty range encloses the 90% confidence interval.

Based again on our smoothed PDM fits from the Monte Carlo simulation, the amplitude of Makemake’s rotational lightcurve is 0.0286 ± 0.0016 mag, where again the error bar corresponds to a 90% confidence interval. The amplitude of a sinusoidal fit to the lightcurve with a period of 7.77 hours is 0.0295 magnitudes, easily consistent to within the error bars, which is not surprising since the PDM lightcurve still closely resembles a sinusoid.

5. Discussion

The rotation period we have determined for 136472 Makemake is in the range of typical rotation periods for Kuiper Belt Objects. There is no evidence for unusual tidal evolution like that of Pluto, whose rotation is tidally slowed by interaction with its moon Charon, nor for a massive collision like the one that appears to be responsible for Haumea’s rapid spin (Ragozzine & Brown 2007). This is consistent with Makemake’s apparent lack of a substantial satellite (Brown et al. 2006b, in press), and with the absence of any evidence for a large impact, in sharp contrast to Haumea.

Somewhat more remarkable is Makemake’s very low photometric amplitude, which is barely a tenth that of Pluto, despite very strong similarities between the two bodies in other respects.

The spectrum of Makemake is nearly identical to that of Pluto, except that the former shows stronger absorption from methane ice. In particular, Makemake shares Pluto’s red color at visible wavelengths (Licandro et al. 2006a,b; Tegler et al. 2007; Brown et al. 2007), in contrast to Eris, which shows strong methane absorption like Makemake, but has a neutral color (Brown et al. 2005). The picture presented by spectra is very consistent: Makemake is red, like Pluto, but Eris has a more neutral color (see especially, Figure 1 of Licandro et al. (2006b)). However, some of the broadband photometry in the literature makes it appear that Eris and Makemake have identical colors. According to Rabinowitz et al. (2007), the $B - V$ colors of Makemake, Eris, and Haumea are 0.828 ± 0.022 and 0.805 ± 0.015 , and 0.646 ± 0.015 , while Buratti et al. (2003) gives $B - V = 0.82 \pm 0.03$ for Pluto. All this is consistent with other sources, except the color of Eris. According to Brown et al. (2005), the $B - V$ color of Eris is 0.71 ± 0.02 , which would make Eris much bluer than Makemake or Pluto, which would then stand out as resembling one another, just as they do in optical spectra. We suggest that though most of the Rabinowitz et al. (2007) photometry is excellent, there may be an error in the B magnitude for Eris, resulting in an incorrect color. This is

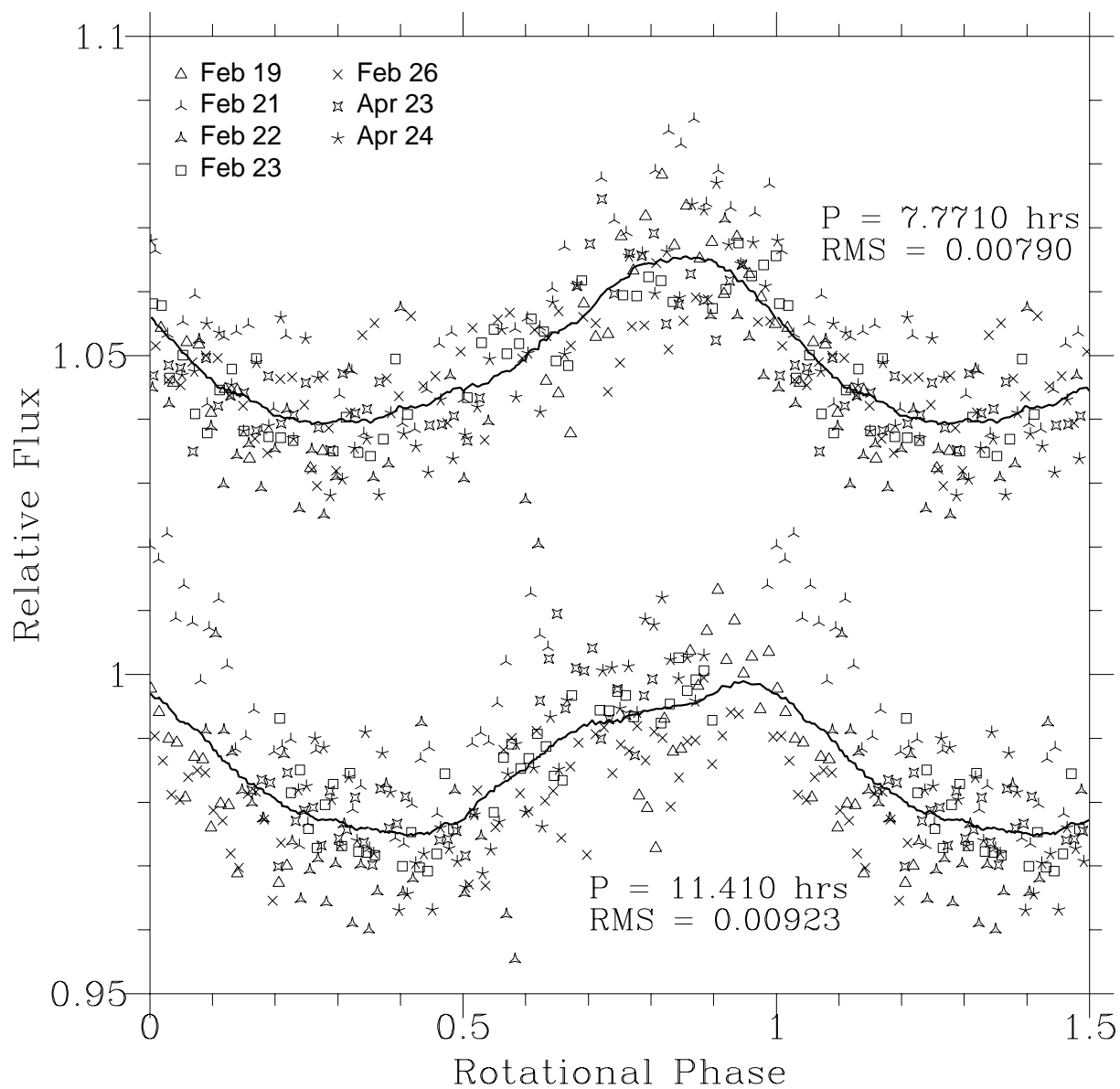


Fig. 8.— Folded lightcurve at the dominant 7.77 hour period compared with the strong alias period of 11.41 hours. Both visually and in terms of the RMS, the 11.41 hour lightcurve is substantially worse.

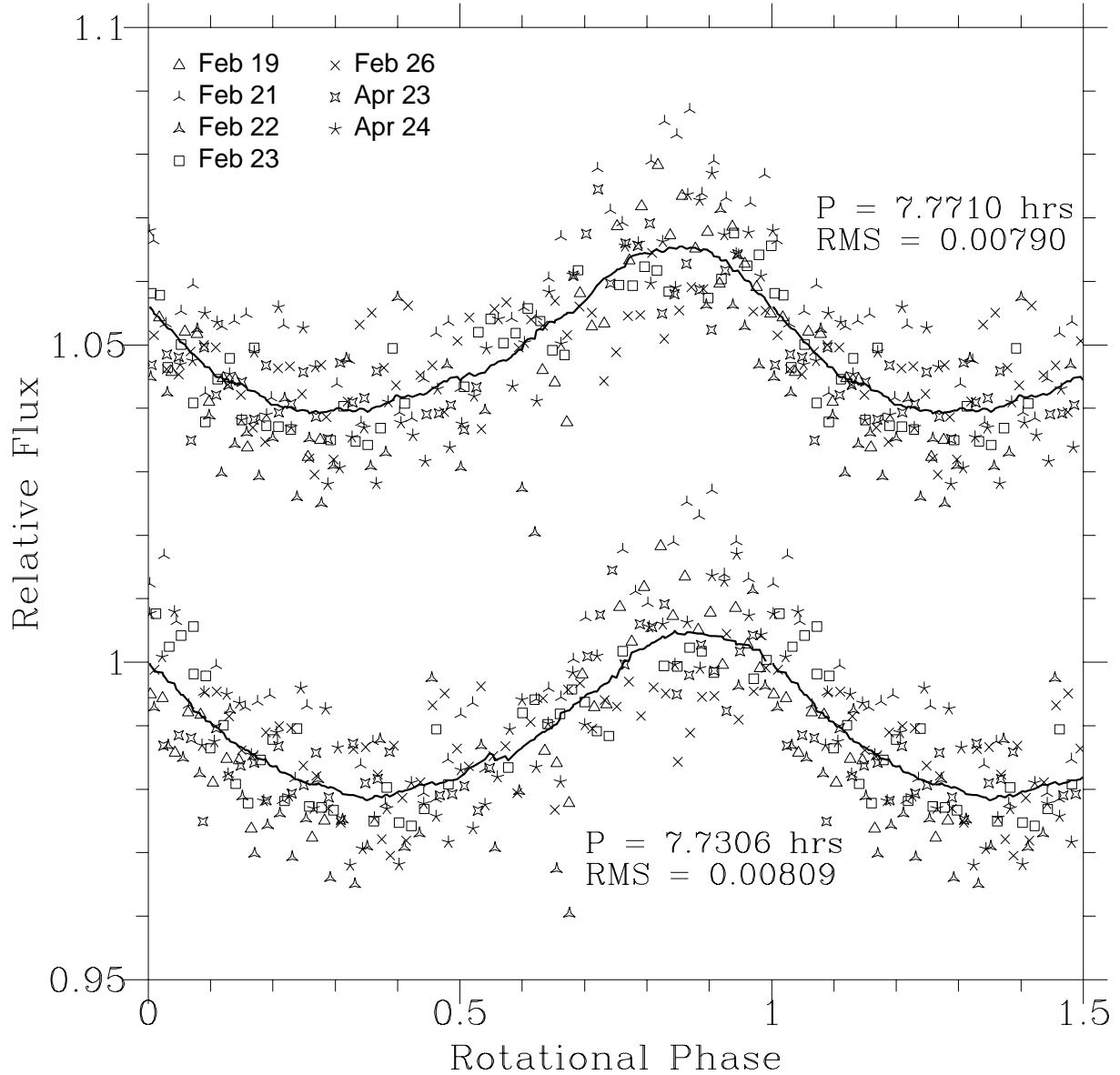


Fig. 9.— Folded lightcurve at the dominant 7.77 hour period compared with the sub-peak period of 7.73 hours. The 7.77 hour lightcurve is noticeably non-sinusoidal, which likely broadened the frequency spread in the periodogram so that the more sinusoidal 7.73 hour period was sometimes identified in the Monte-Carlo simulation. However, the PDM, with no bias towards sinusoids, overwhelmingly preferred the 7.77 hour period.

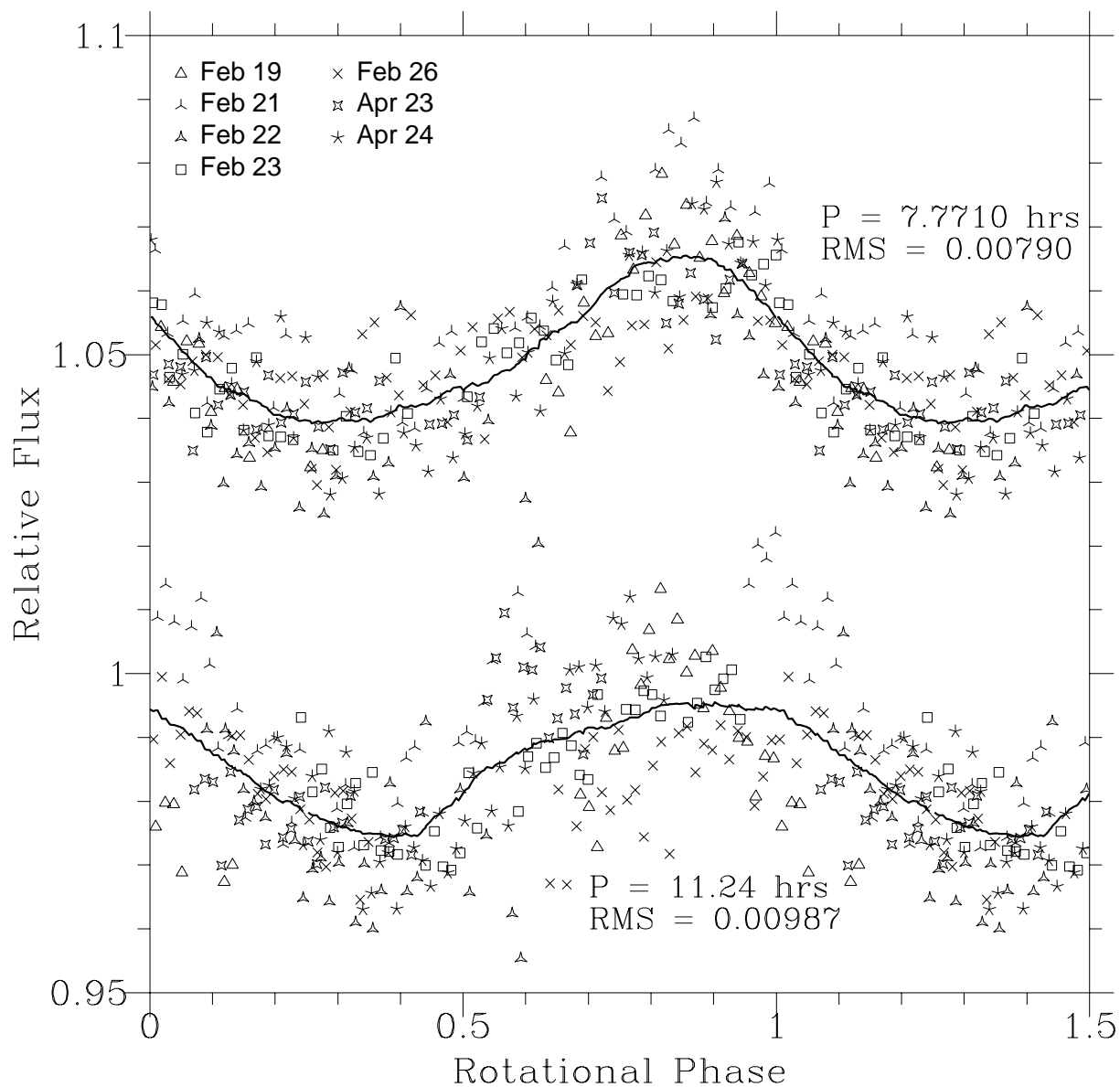


Fig. 10.— Folded lightcurve at the dominant 7.77 hour period compared with the 11.24 hour period preferred by Ortiz et al. (2007). There is no evidence for this period in our data, and the fit is correspondingly bad.

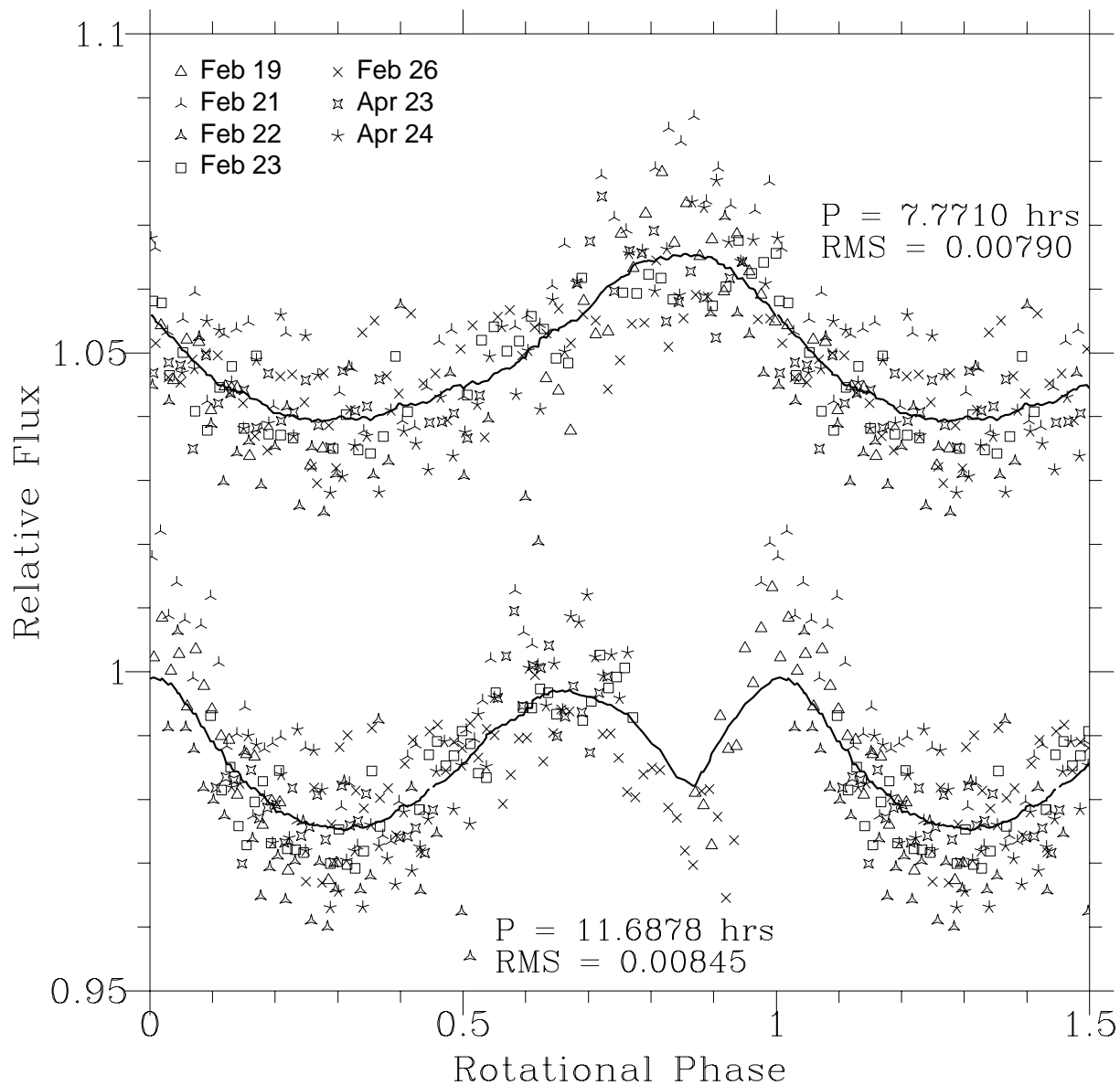


Fig. 11.— Folded lightcurve at the dominant 7.77 hour period compared with the 11.69 hour period identified in our PDM analysis. The jagged shape of the lightcurve and the strong discontinuity between the trends of the Feb 19 and Feb 26 data near phase=0.9 demonstrate the spurious nature of this period.

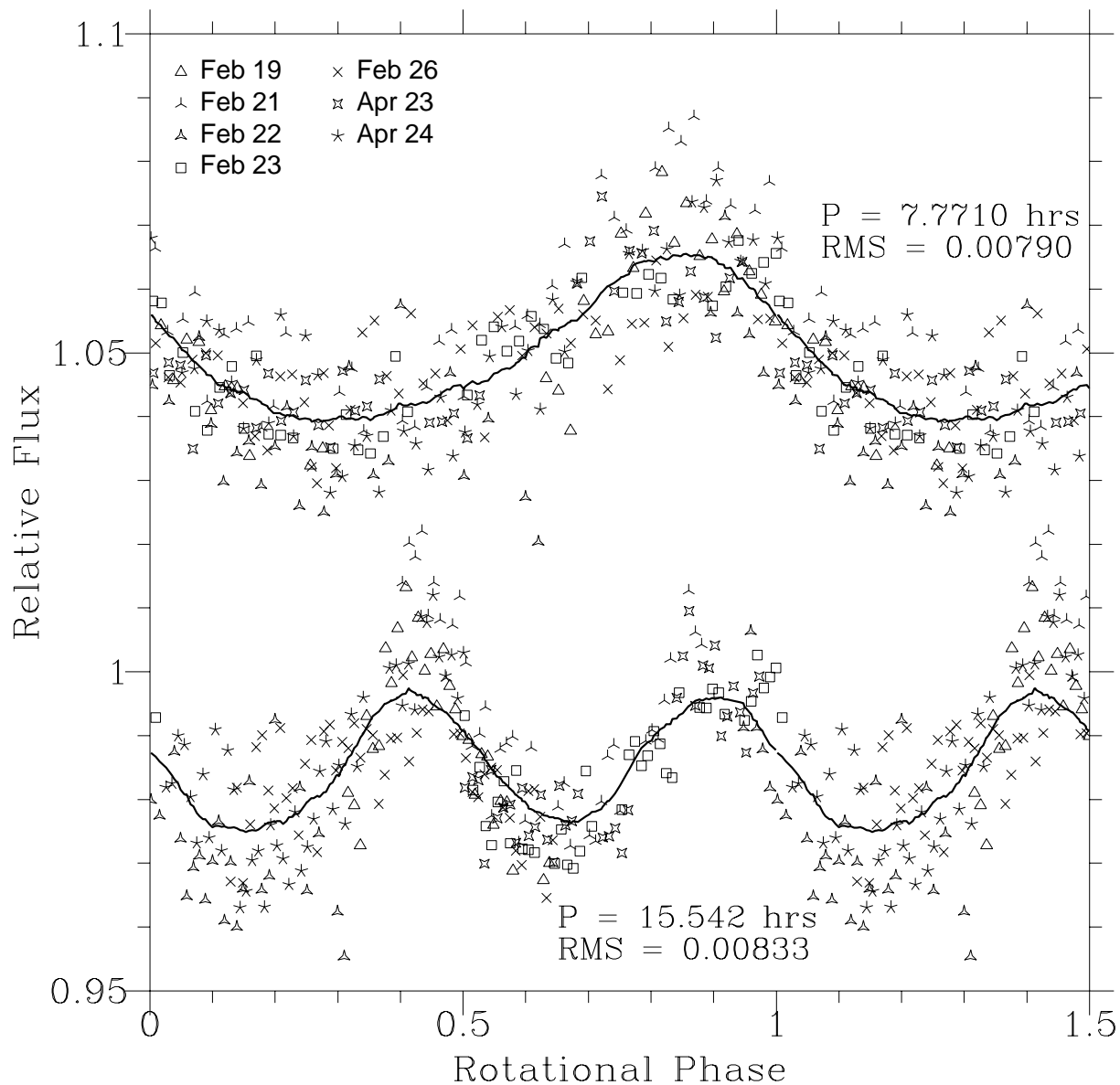


Fig. 12.— Folded lightcurve at the dominant 7.77 hour period compared with the 15.54-hour double-peaked lightcurve. The peaks are almost identical and spaced almost exactly 0.5 apart in phase – requiring an extremely improbable symmetry of albedo features if 15.54 hours were the true period.

suggested by their B band phase slope for Eris, which is negative: an unphysical result. Taking the Brown et al. (2005) value rather than the Rabinowitz et al. (2007) value for the color of Eris resolves the apparent disagreement between the spectra and broadband colors: Makemake and Pluto have very similar colors; Eris is bluer than either.

In terms of albedo, Makemake is midway between Eris and Pluto. Eris has a V band albedo of 0.86 ± 0.07 (Brown et al. 2006a), while that of Makemake is 0.7 ± 0.1 (Brown et al. 2007), and that of Pluto is 0.52 ± 0.03 (Buratti et al. 2003).

The peak-to-valley amplitude of Pluto’s lightcurve is 0.30, 0.26, and 0.21 magnitudes in the B , V , and R bands, respectively (Buratti et al. 2003). The usual explanation for the red color and large photometric amplitude of Pluto is that it has distinct regions covered with dark red tholins which are generated when methane ice is bombarded with UV and ion radiation (Buratti et al. 2003; Brown et al. 2005). This also explains why the amplitude is lower at red wavelengths: the tholins are less dark relative to the surrounding bright ice in the R band than in the B band.

Because of Makemake’s spectral resemblance to Pluto, and in particular its red color, the most obvious a priori assumption would be that it should have similar photometric amplitude. Instead, we find its peak-to-valley amplitude to be approximately nine times smaller, consistent with the results of Ortiz et al. (2007). This is a truly remarkable difference, suggesting either that Makemake’s surface is very uniform and unlike Pluto’s, or that we see it with a nearly pole-on viewing geometry. Brown et al. (2005) suggest that Eris’ neutral color may be due to its larger heliocentric distance (about 90 AU), at which temperatures are sufficiently low for the red tholins to be covered up with a planet-wide frost, which would consist of methane possibly mixed with nitrogen. This would also explain the object’s low photometric variability and high albedo. Ortiz et al. (2007) apply the same global frost theory to explain the low photometric amplitude of Makemake (current heliocentric distance about 52 AU, still considerably greater than Pluto’s), but this explanation seems inconsistent with Makemake’s red, Pluto-like color. Adding to the complication is Makemake’s higher-than-Pluto albedo, which may suggest it is ‘partially frosted’, and indications that methane ice on Makemake may be transparent to centimeter depths (Brown et al. 2007), so that what is below would not necessarily be wholly obscured.

Ortiz et al. (2007) note that the likelihood of both Eris and Makemake being oriented pole-on to us is very low, and argue that most likely there is a common physical reason for the low photometric variability of both objects, i.e. some type of global frost scenario. However, the color difference between Makemake and Eris may present a problem with explaining the low photometric variability of both by the same type of global frost.

We suggest that instead of a global frost, Makemake’s low photometric amplitude may be due to a nearly pole-on viewing geometry. If this is the case, the lightcurve amplitude and shape will change relatively rapidly as the object moves in its orbit. Under this supposition, the lightcurve should look substantially different in twenty years, while if the surface is truly very uniform, the lightcurve will remain essentially unchanged.

A less definitive but still interesting test that could be performed on a shorter timescale is the measurement of Makemake’s lightcurve amplitude at different wavelengths. If the object has Pluto-like dark red patches and is simply being viewed pole-on, the lightcurve amplitude should vary with wavelength just as Pluto’s does. Scaling from Pluto’s wavelength dependent amplitudes and our own value of 0.0286 ± 0.0014 magnitudes for Makemake’s peak-to-valley V -band photometric amplitude, we would predict a B band amplitude of 0.0330 mag and an R band amplitude of 0.0231 magnitudes. This difference could easily be detected with photometry as precise as that we have presented herein. If the B band lightcurve did not show a markedly larger amplitude than the R band, the hypothesis that Makemake is a pole-on Pluto analog could be dismissed. We note that Ortiz et al. (2007) determined an R band lightcurve amplitude of 0.03 ± 0.01 magnitudes for Makemake, but given the large uncertainty, this does not rule out the value we predict for a pole-on Pluto scenario.

We have obtained some of the most precise time-series photometry ever acquired for a Kuiper Belt object. A similar project performed on Eris might yield the first confident determination of its rotation period as well. It is even possible that similar work could be extended to a precise measurement of Eris’ lightcurve amplitudes in the B , V , and R bands. This would allow a test of the theory that Eris’ red tholins are covered up with a global methane frost: if they are, the lightcurve amplitude should be the same at all wavelength bands.

6. Conclusion

We have obtained precise, well sampled time-series photometry of the dwarf planet 136472 Makemake, formerly known as 2005 FY9, and have determined accurate values for its rotation period and rotational lightcurve amplitude. Its rotation period is 7.7710 ± 0.0030 hours, with 90% confidence. The amplitude of its rotational lightcurve is 0.0286 ± 0.0016 magnitudes.

Makemake’s rotation period is in the typical range for Kuiper Belt Objects, unlike those of Pluto and Haumea, which have been dramatically altered by tidal evolution and a giant impact, respectively.

The very low photometric amplitude of Makemake is surprising given the much larger variability of Pluto, and the spectral similarity between the two objects. Makemake may have an extremely uniform surface, but the previous suggestion of a global methane frost due to the low temperatures encountered at large heliocentric distances appears inconsistent with the object’s Pluto-like red color. Our observations are also consistent with a Pluto-like variegated surface combined with a nearly pole-on viewing geometry.

We have demonstrated that, given a 1.5 meter telescope and a high quality CCD in good weather, very careful data reduction can yield considerably more precise relative photometry of bright Kuiper Belt Objects than has generally been published in the past. Similar techniques applied to Eris might well result in a confident determination of its rotation period, which has

so far been elusive. Observing Makemake itself at different wavelength bands could determine whether or not its lightcurve is dominated by Pluto-like deposits of dark red tholins – if so, the photometric amplitude should be lower in the *R* band and greater at *B*. The same type of extremely precise multi-wavelength observations applied to Eris could test the theory that the red deposits that probably exist on its surface are covered with a uniform methane frost – if so, the lightcurve amplitude should be wavelength independent. Time series photometry of the precision we present here represents a potentially powerful tool for the study of large objects in the Kuiper Belt.

7. Acknowledgements

This research has made use of the SIMBAD online database, operated at CDS, Strasbourg, France.

This research has made use of the VizieR online database (see Ochsenbein et al (2000)).

This research has made extensive use of information and code from Press et al. (1992).

Facilities: 61” Kuiper

REFERENCES

- Brown, M. E., Trujillo, C.A. & Rabinowitz, D. L. 2005, ApJ635L, 97
- Brown, M. E.; Schaller, E. L.; Roe, H. G.; Rabinowitz, D. L.; Trujillo, C. A. 2006, ApJ, 643L, 61
- Brown, M. E., van Dam, M. A., Bouchez, A. H., Le Mignant, D., Campbell, R. D., Chin, J. C. Y., Conrad, A., Hartmat, S. K., Johansson, E. M., Lafon, R. E., Rabinowitz, D. L., Stomski, P. J., Summers, D. M., Trujillo, C. A., & Wizonowich, P. L. 2006, ApJ, in press
- Brown, M. E., Barkume, K. M., Blake, G. A., Schaller, E. L., Rabinowitz, D. L., Roe, H. G., & Trujillo, C. A. 2007, AJ133, 284
- Bryden, G., Beichman, C. A., Trilling, D. E., Rieke, G. H., Holmes, E. K., Lawler, S. M, Stapelfeldt, K. R., Werner, M. W., Gautier, T. N., Blaylock, M. Gordon, K. D., Stansberry, J. A., & Su, K. Y. L. 2006, ApJ, 636, 1098
- Buratti, B. J., Hillier, J. K., Heinze, A., Hicks, M. D., Tryka, K. A., Mosher, J. A., Ward, J., Garske, M., Young, J. & Atienza-Rosel, J. 2003, Icarus, 162, 171
- Chamberlain, M., Sykes, M. V., & Esquerdo, G. A. 2007, Icarus, 188, 451
- Cox, A. N. 2000, Allen’s Astrophysical Quantities (Fourth Edition; New York, NY: Springer-Verlag New York, Inc.)

- Duffard, R., Ortiz, J. L., Santos Sanz, P., Mora, A., Gutiérrez, P. J., Morales, N., & Guirado, D. 2008, *A&A*, 479, 877
- Gaudi, B. S., Stanek, K. Z., Hartman, J. D., Holman, M. J., & McLeod, B. A. 2005, *ApJ*, 629, L49
- Gomes, R., Levison, H. F., Tsiganis, K., & Morbidelli, A. 2005, *Nature*, 435, 466G
- Li, J., McFadden, L. A., Thomas, P. C., Mutchler, M., Parker, J. W., Young, E. F., Russel, C. T., Sykes, M. V., & Schmidt, B. 2007, *DPS*, 39.3011.L
- Licandro, J., Pinilla-Alonso, N., Pedani, M., Oliva, E., Tozzi, G. P., & Grundy, W. M. 2006, *A&A*, 445, L35
- Licandro, J.; Grundy, W. M.; Pinilla-Alonso, N.; Leisy, P. 2006, *A&A*, 458L, 5
- Ochsenbein, F., Bauer, P. & Marcout, J. 2000, *ApJS*, 143, 230
- Ortiz, J. L., Gutiérrez, P. J., Sota, A., Casanova, V., & Teixeira, V. R. 2003, *A&A*, 409, L13
- Ortiz, J. L., Gutiérrez, P. J., Santos-Sanz, P., Casanova, V., & Sota, A. 2006, *A&A*, 447, 1131
- Ortiz, J. L., Santos-Sanz, P., Gutiérrez, P. J., Duffard, R. & Aceituno, F. J. 2007, *A&A*, 468, L13
- Press, W. H., Teukolsky, S.A., Vetterling, W. T., & Flannery, B. P. 1992, *Numerical Recipes in C* (Second Edition; New York, NY: Cambridge University Press) *PASP*, 113, 1420
- Rabinowitz, D. L., Kristina, B., Brown, M. E., Roe, H., Schwartz, M., Tourtellotte, S., Trujillo, C. 2006, *ApJ*, 639,1238
- Rabinowitz, D. L., Schaefer, B. E., & Tourtellotte, S. W. 2007, *AJ*, 133, 26
- Ragozzine, D., & Brown, M. E., *AJ*, 134, 2160
- Sheppard, S. S., & Jewitt, D. C., *AJ*, 124, 1757
- Sheppard, S. S. 2007, *AJ*, 134, 787
- Stansberry, J., Grundy, W., Brown, M., Cruikshank, D., Spencer, J., Trilling, D., & Margo, J. 2007, *ArXiv e-prints*, astro-ph/0702538v2
- Stellingwerf, R. F. 1978, *ApJ*, 224, 953
- Tegler, S. C.; Grundy, W. M.; Romanishin, W.; Consolmagno, G. J.; Mogren, K.; Vilas, F. 2007, *AJ*133, 526
- Trilling, D. E., & Bernstein, G. M. 2006, *AJ*, 121, 1149
- van Dokkum, P. G. 2001, *PASP*, 113, 1420